

Article

Effect of Nitrogen Doping on Tribological Properties of Ta₂O₅ Coatings Deposited by RF Magnetron Sputtering

Rui Chao ^{1,2,3}, Haichao Cai ^{1,2,3}, Hang Li ^{1,2} and Yujun Xue ^{1,2,3,*}¹ School of Mechatronics Engineering, Henan University of Science and Technology, Luoyang 471003, China² Henan Key Laboratory for Machinery Design and Transmission System, Luoyang 471003, China³ Longmen Laboratory, Luoyang 471000, China

* Correspondence: yjxue@haust.edu.cn; Tel.: +86-379-64278961

Abstract: Ta₂O₅ was deposited on quartz glass and Si substrates as a protective coating. The inherent RF magnetron sputtering power of 140 W was maintained during the deposition process. During the deposition process, amounts of 5%, 10%, and 15% of N₂ were injected, and the total sputtering gas (N₂+Ar) flow was kept at 40 sccm. The microstructure and surface morphology of the coatings were characterized, and the friction and wear experiments of the coatings were carried out. The results show that the coatings' surface is smooth and the main chemical compositions are Ta, O, and N. The maximum average roughness of the coatings was prepared by pure argon sputtering. It is proved that the introduction of N₂ reduces the surface roughness of the coatings and increases the surface hardness and elastic modulus of the coatings. Adhesive wear and brittle fracture are the two main wear forms of coatings. The wear debris is mainly composed of columnar particles and a flake structure.

Keywords: magnetron sputtering; Ta₂O₅; TaN; friction; wear; surface morphology



Citation: Chao, R.; Cai, H.; Li, H.; Xue, Y. Effect of Nitrogen Doping on Tribological Properties of Ta₂O₅ Coatings Deposited by RF Magnetron Sputtering. *Materials* **2022**, *15*, 8291. <https://doi.org/10.3390/ma15238291>

Academic Editors: Claudia Barile and Gilda Renna

Received: 25 October 2022

Accepted: 16 November 2022

Published: 22 November 2022

Publisher's Note: MDPI stays neutral with regard to jurisdictional claims in published maps and institutional affiliations.



Copyright: © 2022 by the authors. Licensee MDPI, Basel, Switzerland. This article is an open access article distributed under the terms and conditions of the Creative Commons Attribution (CC BY) license (<https://creativecommons.org/licenses/by/4.0/>).

1. Introduction

Compared with fossil energy, the power generation conversion rate is low, with high pollution and non-renewable disadvantages. Because it is clean and renewable, photovoltaic power generation has become the new energy that is widely used in human life and industry. Photovoltaic power generation is considered to have great potential in the power industry and has become a hot topic at home and abroad in recent years [1]. Studies have shown that the global solar photovoltaic market has developed rapidly with a growth rate of 50% over the past decade [2,3]. Because the actual working environment of photovoltaic cells often appears as dust, rain, and other bad weather, in order to avoid damage to photovoltaic cell components, high transmittance glass is commonly used as the cover protection component part [4,5]. Dust and gravel particles generate frictional wear when they accumulate on the surface of the glass cover due to wind factors, and this situation not only reduces the light transmission of the glass cover [6], but also affects the photovoltaic cell's photoelectric conversion efficiency [7,8]. It is reported that in the Saudi region, within a few months, due to dust deposition, photovoltaic cell system power generation efficiency was reduced by more than 30% [9]. Many researchers have carried out a lot of research on the problem of friction and the wear of glass cover plates caused by dust accumulation. It has become a common method to apply functional coating on equipment surfaces in recent years, such as transparent coating [10], conductive coating [11], wear-resistant coating [12,13], and lubricating coating [14,15].

Transition metal nitride coatings are used as multifunctional coatings in many fields due to their high hardness, high wear resistance, chemical inertness, and high temperature stability. TaN has attracted increasing attention due to its excellent chemical and physical properties. It is widely used as a hard coating, wear-resistant coating, and integrated circuit diffusion layer [16]. Much of the research literature has focused on physical vapor

deposition (PVD) technology, with pure Ta as a target, after the introduction of N_2 and a tantalum ion reaction to form the TaN coating. CHEN R et al. used DC magnetron sputtering technology, with pure tantalum as a target, and found that a columnar structure exists in a single layer TaN coating [17]. A multilayer TaN coating has a higher hardness and lower friction coefficient than a single layer TaN coating. SEMPAH I et al. found that grain refinement by boron addition improves the hardness of the TaN coating, and the friction coefficient decreases with the increase in boron content [18]. SERNA-MANRIQUE M D et al. sputtered TaN coatings on 304 stainless steel items in a N_2/Ar atmosphere [19]. It was found that the power has a direct relationship with the formation of specific grains in the coating, which further affects the corrosion resistance of the coating.

Ta_2O_5 coatings are often used as high-performance materials in optical devices [20] due to their good optical properties, thermal stability [21] and chemical stability [22] in the visible and near-infrared regions, and high refractive index [23]. Ta_2O_5 also has good mechanical properties such as wear resistance [24] and high hardness [25], and can be used as a protective coating. According to the relevant literature, Ta metal oxide Ta_2O_5 was proposed as the target.

In our previous study, the optical properties of Ta_2O_5 coatings prepared under sputtering powers of 100 W, 120 W, 140 W, 160 W, and 180 W were studied. The results showed that the transmittance of the coatings was high when the sputtering power was 140 W, indicating that the morphology was uniform and smooth. In order to further improve the mechanical properties of the coatings prepared under this sputtering power condition, N_2 was introduced during the preparation process to study the effect of the N_2 flow rate on the coating's quality. In this paper, the mechanical properties and friction and wear properties of coatings under different nitrogen/argon ratios of 40Ar, 36Ar–4 N_2 , 34Ar–6 N_2 , and 32Ar–8 N_2 were studied. The purpose was to analyze the relationship between the sputtering gas flow rate and the mechanical properties of the coatings. In addition, the composition and roughness of the films were characterized.

2. Materials and Methods

The Ta_2O_5 thin films were prepared by RF magnetron sputtering technique through JGP045CA (Shenyang Scientific Instrument Co., Ltd. Xinyuan Street, Hunnan District, Shenyang, China) sputtering system [26]. The substrate was highly transparent quartz glass (10 mm × 10 mm × 2 mm) and N<111> type silicon wafer (7 mm × 7 mm × 0.5 mm). The samples were ultrasonically cleaned with acetone, anhydrous ethanol, and deionized water for 15 min with SCIENTZ-450 (Xinzhi Freeze-drying Equipment Co., Ltd. Jiao Chuan Street, Zhenhai District, Ningbo, China) equipment before deposition, dried with compressed air, and prepared for use. The back-bottom vacuum was pumped to below 5×10^{-4} Pa, and the deposition pressure was 0.8 Pa. The total gas flow rate for deposition was kept constant at 40 sccm (10%, 15%, and 20% for $N_2/(N_2+Ar)$ in the experiment, respectively). The target material was Ta_2O_5 of 99.99% purity ($\phi 30 \times 3$ mm, Beijing Goodwill Metal Technology Development Co., Ltd. Dazhong Temple, Haidian District, Beijing, China). The deposition temperature was room temperature, the sputtering power was 140 W, and the substrate rotation speed was 10 rpm (no negative bias). A clean target surface was obtained by glow discharge pre-sputtering for 10 min before deposition, and the deposition time was 45 min.

A ball on disc tribometer used for wear and friction tests was used to evaluate the friction and wear characteristics of the composite coating samples and ceramic balls at room temperature (HT-1000, Lanzhou Zhongke Kaihua Technology Development Co., Ltd. Nanchang Road, Chengguan District, Lanzhou, China). A ball on disc tribometer used for wear and friction tests is shown in Figure 1. Ceramic balls ($\phi 5$ mm) were pressed against the sample surface during sliding with a constant load of 2 N. The relative rotation of the sample and the ceramic was maintained at 100 rpm until the film on the sample surface failed. The microhardness (H) and Young's modulus (E) of the sample film were tested by applying a load of 50 mn to the single crystal silicon wafer using a nanoindentation ZDT075-075 (Liansheng Technology Co., Ltd. Xiaolan Economic Development Zone, Jinsha

Third Road, Nanchang, China) equipped with a diamond indenter. The nanoindentation depth should be less than 10% of the coating thickness. Scanning electron microscopy (SEM, Zeiss Sigma 300, Jena, Germany) was used to analyze the surface morphology and abrasion marks on the sample surface before and after the friction test, and to obtain an approximation of the film deposition thickness from the cross-sectional morphology of the coatings. Determination of film composition by energy spectrum of the sample surface was obtained by an energy dispersive spectrometer (Smart EDX). The surface morphology of the sample was obtained using an atomic force microscope (AFM, Bruker Dimension Icon, Ettlingen, Germany). At the same time, the surface roughness (Ra) and root mean square (RMS) of the samples were obtained.

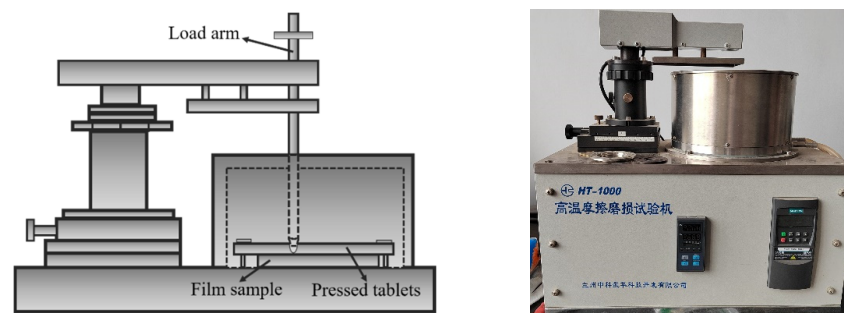


Figure 1. A ball on disc tribometer is used for wear and friction tests.

3. Results

The XRD patterns of Ta₂O₅ coatings deposited under different flow rates of N₂ and Ar are shown in Figure 2. XRD was used to analyze the phase structure of Ta metal composite coating deposited on the glass base substrate. It can be seen from Figure 2 that the coatings are amorphous when the sputtering gas conditions are 40Ar, 36Ar–4N₂, 34Ar–6N₂, and 32Ar–8N₂, respectively. Because a large number of Ta atoms are released from the target, they are freely mixed with argon ion radicals and nitrogen ions in the chamber. One part of the Ta atom recombines with the oxygen atom to form a tantalum metal oxide, and the other part combines with the nitrogen atom to form a tantalum metal nitride. As a result, the dynamic energy of the Ta metal particles reaching the substrate is reduced, and the crystal structure cannot be formed by orderly arranging of the particle positions.

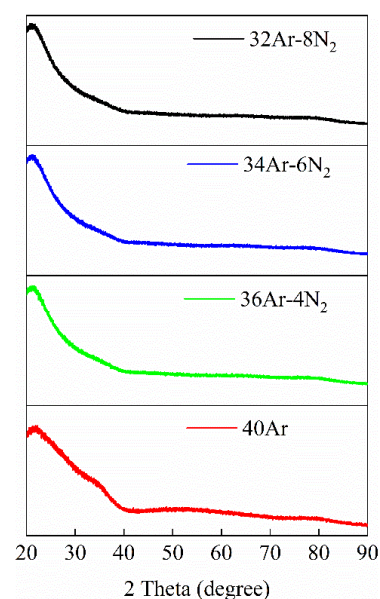


Figure 2. XRD spectra of Ta₂O₅ coatings deposited at sputtering power of 140 W with different N₂ and Ar fluxes.

Since the change in the N_2 flow rate will affect the microstructure of the sample coating, the surface roughness of the sample was characterized by atomic force microscopy (AFM). The 2D and 3D morphology of the coatings' surface roughness is shown in Figure 3. The scanning area is $3 \mu\text{m} \times 3 \mu\text{m}$. The coatings were prepared under pure argon sputtering conditions as shown in Figure 3a. The sputtered particles accumulate into a pyramid shape on the coatings' surface, and there are broad peaks. The coatings prepared under mixed gas sputtering conditions are shown in Figure 3b–d. The sputtered particles on the surface of the coatings accumulate into the columnar structure. The peak decreases with the increase in the N_2 flow rate. The maximum peaks on the surface of each coating are 6.7 nm, 2.0 nm, 1.7 nm, and 1.5 nm, respectively.

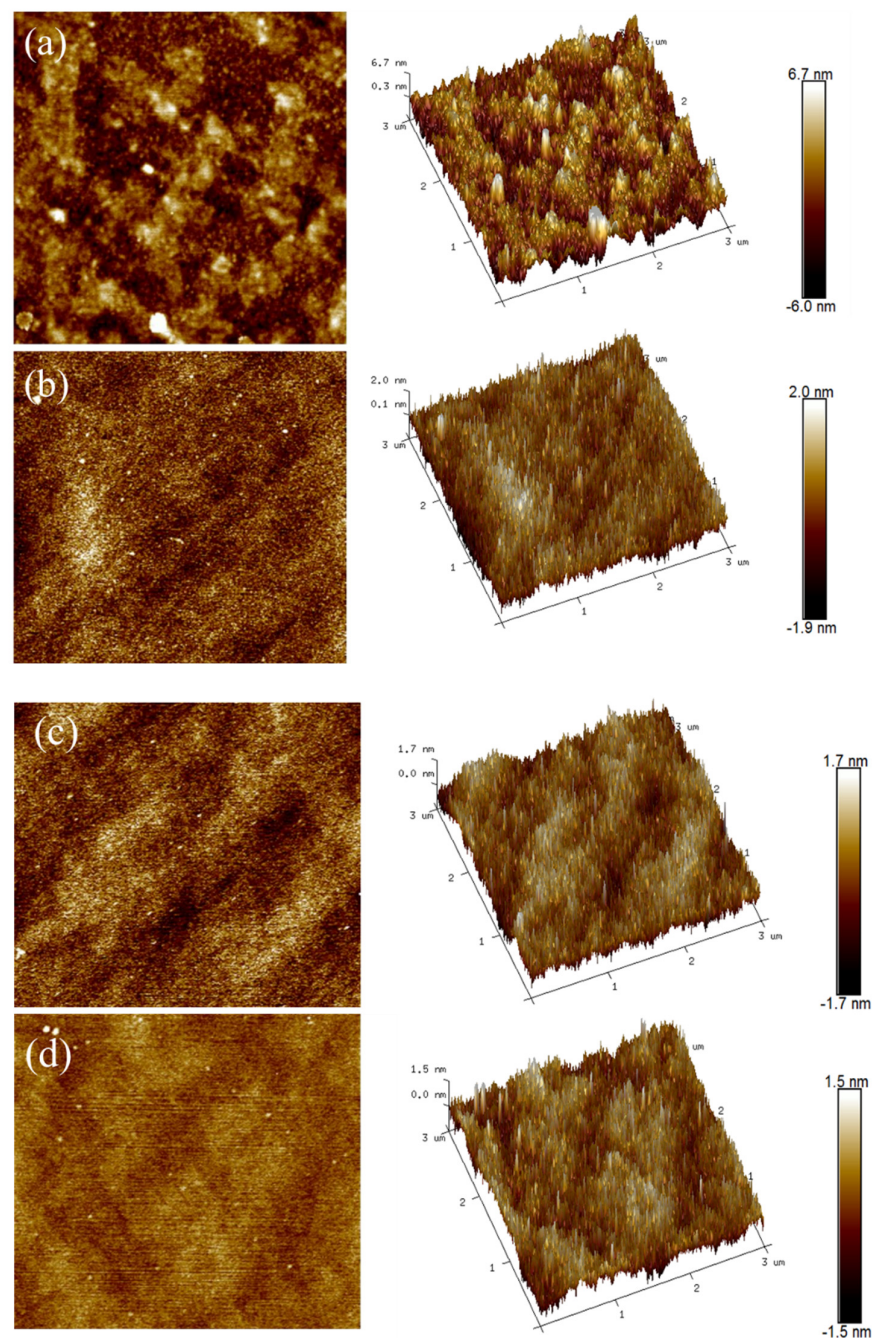


Figure 3. Surface roughness 2D and 3D AFM images of Ta_2O_5 coatings were prepared under different sputtering gas conditions. (a) 40Ar, (b) 36Ar–4 N_2 , (c) 34Ar–6 N_2 , (d) 32Ar–8 N_2 .

The roughness of coating samples prepared under different sputtering gas conditions was measured. The average roughness (Ra) and the root mean square (RMS) of the coatings' surfaces are shown in Table 1 and Figure 4. The average roughness of the coating samples is nanoscale, indicating that the coatings' surfaces are smooth. The mean values of Ra and RMS of the coating samples prepared under pure argon sputtering conditions are much larger than those of the coating samples prepared under mixed gas sputtering conditions. After N₂ was introduced, the Ra value and RMS value of the coating surface decreased with the increase in the N₂ flow rate.

Table 1. The average surface roughness of Ta₂O₅ coatings prepared under different sputtering gas conditions was measured by AFM.

Sample	40Ar	36Ar-4N ₂	34Ar-6N ₂	32Ar-8N ₂
Ra (nm)	1.48	0.429	0.382	0.347
RMS (nm)	1.86	0.551	0.482	0.437

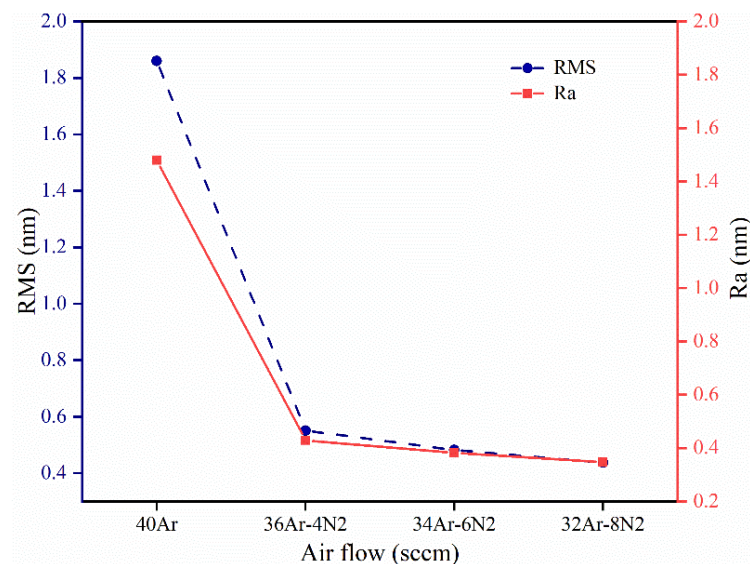


Figure 4. Surface Ra and RMS values of Ta₂O₅ coatings prepared under different sputtering gas conditions.

In order to observe the surface morphology and element distribution of the coating sample after N₂ was introduced, the SEM and EDS spectra of the Ta₂O₅ coating prepared under different sputtering gas conditions are shown in Figure 5. Figure 5a shows that there is a large area of the convex part formed by the accumulation of sputtered particles on the surface of the coating, and the size of the convex part is larger. Figure 5b–d show that only a few bulges were formed by the accumulation of sputtered particles on the coating surface. The changing trend of the surface morphology and roughness of the coatings are basically consistent with those of Figures 3 and 4 and Table 1. The AFM and SEM surface morphology analysis of the coatings shows that the passage of N₂ can change the sputtered particles' stacking structure and optimize the surface quality of the coatings. The deposition thickness of the coatings was 685.4 nm, 437.6 nm, 433.8 nm, and 337.8 nm after SEM scanning of the cross-section of the coatings when the sputtering gas flow rate was 40Ar, 36Ar-4N₂, 34Ar-6N₂, and 32Ar-8N₂. Cross-sectional SEM images of the Ta₂O₅ coatings prepared under different sputtering gases are shown in Figure 6.

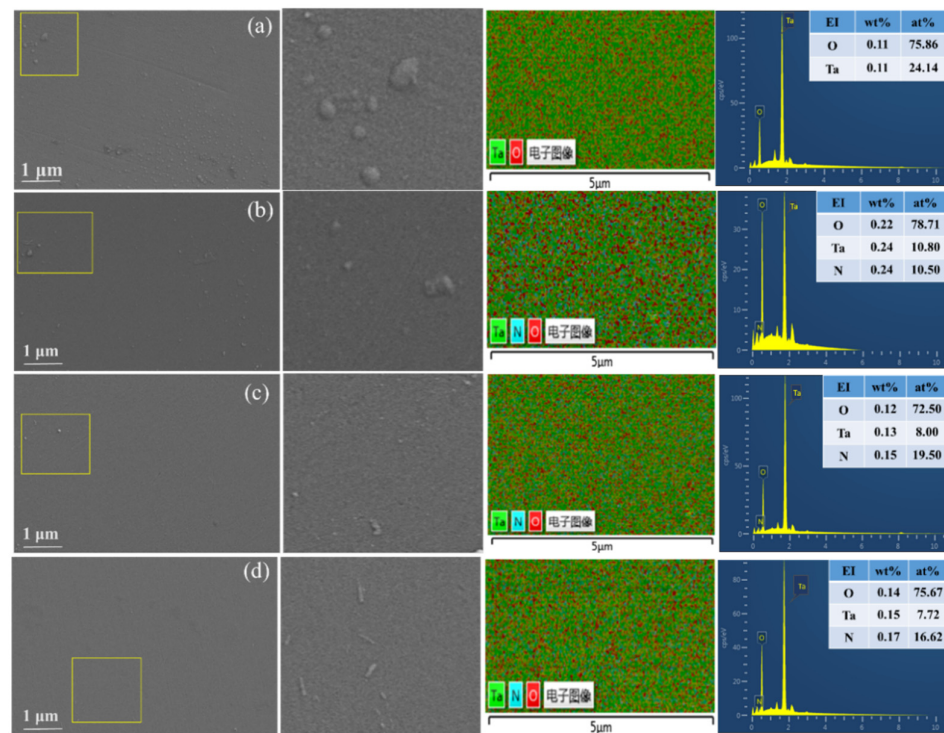


Figure 5. SEM images and EDS spectra of Ta_2O_5 coatings prepared under different sputtering gas conditions. (a) 40Ar, (b) 36Ar–4N₂, (c) 34Ar–6N₂, (d) 32Ar–8N₂.

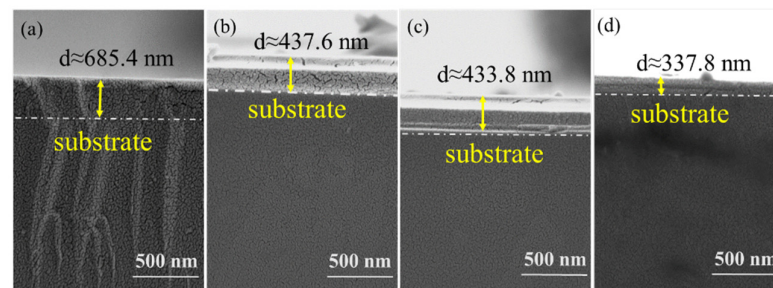


Figure 6. Cross-sectional SEM images of Ta_2O_5 coatings prepared under different sputtering gases. (a) 40Ar, (b) 36Ar–4N₂, (c) 34Ar–6N₂, (d) 32Ar–8N₂.

The average concentration and distribution of elements in the coating samples were obtained by EDS, as shown in the table and energy spectrum in Figure 5a–d. The table in Figure 5a shows no nitrogen atoms in the coatings. The table in Figure 5b–d shows a gradual increase in the content of nitrogen atoms, consistent with changing sputtering gas conditions during preparation. The EDS spectrum showed that Ta, O, and N elements were evenly distributed in the coatings.

Hardness (H) and elastic modulus (E) are two important mechanical properties of materials. The ratio of H/E and H^3/E^2 is a parameter reflecting the ability of materials to resist plastic deformation, which is usually used to evaluate the toughness and wear resistance of materials [27,28]. The surface hardness and elastic modulus of Ta_2O_5 coatings prepared under different sputtering gas conditions are shown in Table 2. It can be seen from the data in the table that the hardness and elastic modulus of the coating samples prepared under pure argon sputtering conditions are smaller than those prepared under mixed gas sputtering conditions. The effect of the nitrogen–argon gas flow ratio on surface hardness and the elastic modulus of coatings showed that they both increased with increasing nitrogen flow. The increase in the nitrogen flow rate makes more nitrogen ions combine with tantalum ions to form a thicker nitride coating.

Table 2. Surface hardness and elastic modulus of Ta₂O₅ coatings were prepared under different sputtering gas conditions.

Sample	Hardness GPa	Young's Modulus GPa	H/E	H ³ /E ²
40Ar	8.463	106.7	0.079	0.0540
36Ar-4N ₂	12.371	108.1	0.114	0.1620
36Ar-6N ₂	14.401	112.4	0.128	0.2363
32Ar-8N ₂	15.207	117.8	0.129	0.2534

The friction coefficient curves of the Ta₂O₅ coatings prepared under different sputtering gases are shown in Figure 7. The fluctuation of the friction curve of the coatings prepared at a sputtering gas flow rate of 40Ar is the smallest. The fluctuation range of the friction coefficient curve of the coating samples is the largest when the sputtering gas flow rate is 36Ar-4N₂. The fluctuations of the friction curves of the coating samples prepared at sputtering gas flow rates of 34Ar-6N₂ and 32Ar-8N₂ are relatively small. The average friction coefficient curves of the coatings were: 0.230, 0.415, 0.249, and 0.258.

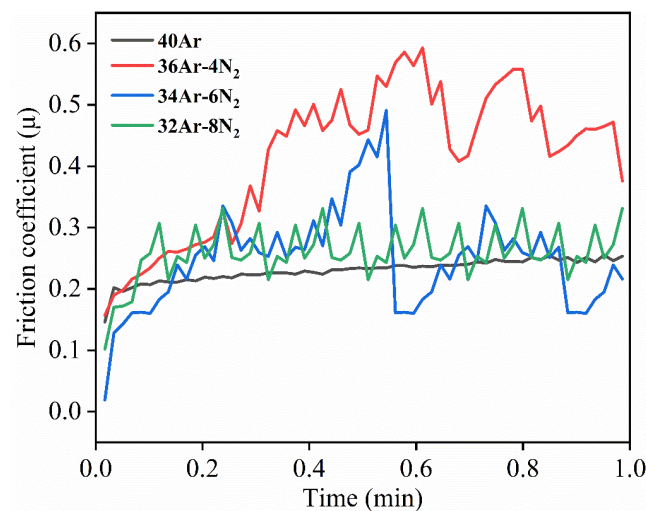


Figure 7. Friction coefficient of Ta₂O₅ coatings prepared under different sputtering gas conditions.

In order to understand the main reasons affecting the friction coefficient of the coating samples and explore the friction and wear mechanism of the coatings, the coatings' wear marks and debris were emphatically analyzed. The SEM images of the wear scar morphology of Ta₂O₅ coating samples prepared under different sputtering gas flow rates (magnification of 5 K and 10 K) are shown in Figure 8. Figure 8a shows that there is no spalling and brittle fracture in the wear scar when the sputtering gas is 40Ar, and a large area of the coatings transfer layer appears on the surface of the wear scar. Figure 8b shows that a small amount of the coatings on the surface of the wear scar peels off, transfers, and then restacks to appear as bulges when the sputtering gas is 36Ar-4N₂, which is also the main reason for the large fluctuation in the friction curve. Figure 8c shows that the wear track exhibits brittle fracture and spalling when the sputtering gas is 34Ar-6N₂. The crack may be the position where the friction curve of the coating fluctuates the most. There is no large area accumulation bulge in coating transfer, which is basically consistent with the fluctuation in the friction curve. Figure 8d shows that a large area of spalling appears on the wear scar when the sputtering gas is 32Ar-8N₂.

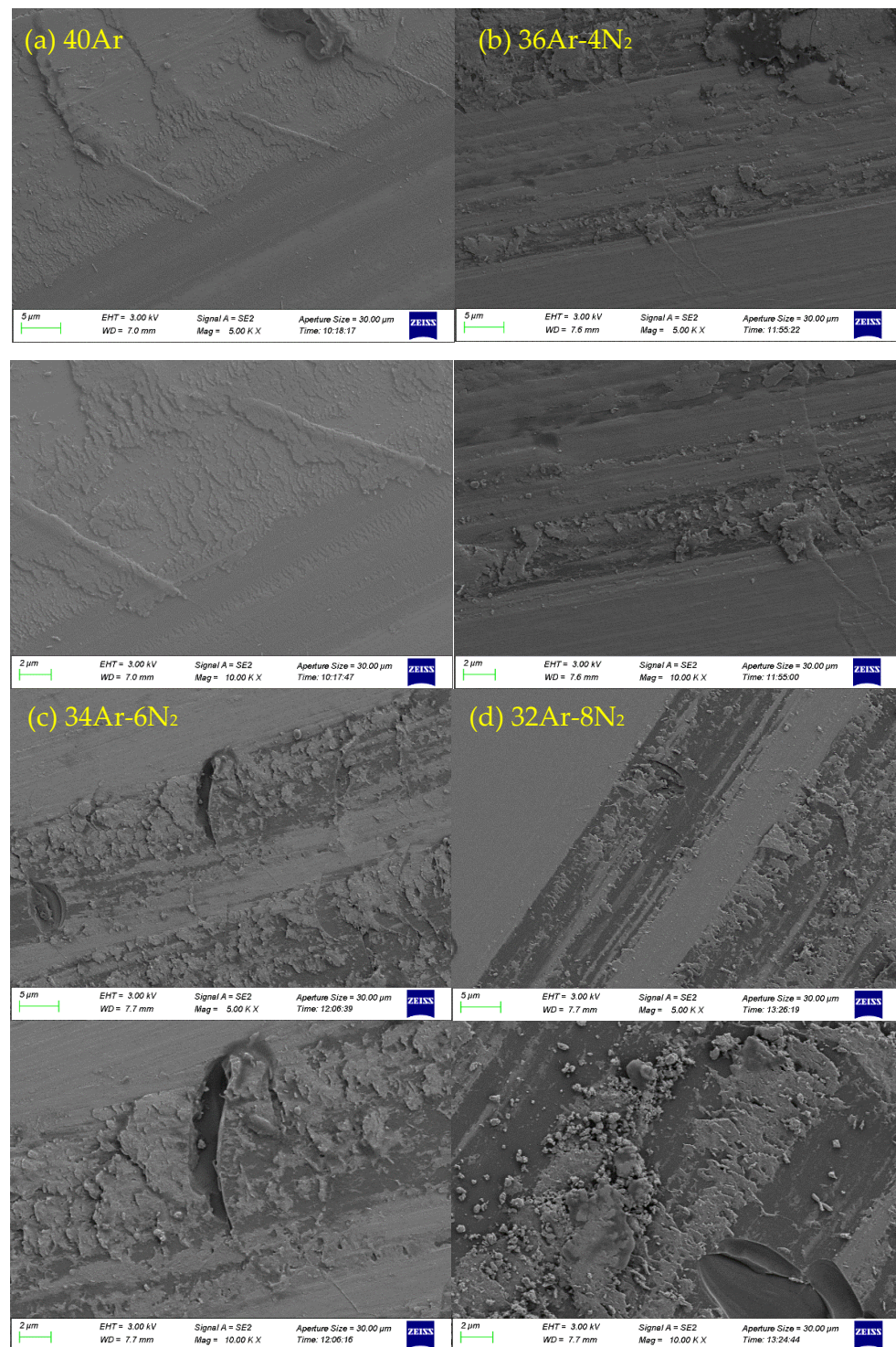


Figure 8. SEM images of wear scar morphology of Ta_2O_5 coatings prepared under different sputtering gas conditions. (a) 40Ar, (b) 36Ar-4N₂, (c) 34Ar-6N₂, (d) 32Ar-8N₂.

Local amplification of the wear track (magnification 20 K). The wear debris morphology in the wear track is shown in Figure 9. It can be seen that the wear debris of the coating samples prepared under different sputtering gas conditions is very different. Figure 9a shows that the wear debris is mainly composed of fine columnar particles when the sputtering gas is 40Ar. Figure 9b shows that the wear debris is mainly composed of blocks and flakes when the sputtering gas is 36Ar-4N₂. Figure 9c shows that the wear debris is mainly composed of columnar particles and flakes when the sputtering gas is 34Ar-6N₂. Figure 9d

shows that the wear debris is mainly composed of larger particles when the sputtering gas is 32Ar–8N₂.

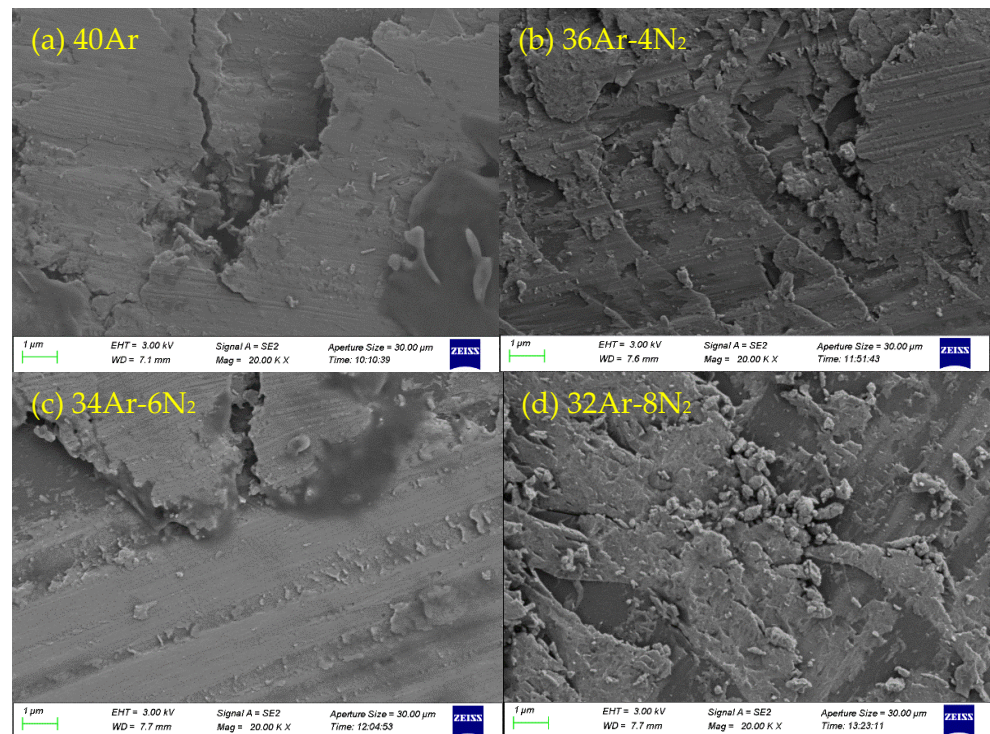


Figure 9. Wear debris morphology of Ta₂O₅ coatings prepared under different sputtering gas conditions. (a) 40Ar, (b) 36Ar–4N₂, (c) 34Ar–6N₂, (d) 32Ar–8N₂.

4. Conclusions

Ta₂O₅ coatings were prepared by RF magnetron sputtering under different sputtering gas conditions. The microstructure and mechanical properties of the coatings were evaluated by XRD, AFM, SEM, EDX, a nanoindenter, and a friction and wear tester. The results show that the prepared coating samples are amorphous film. The coating samples are mainly composed of the three elements, Ta, N, and O, and these are evenly distributed in the coatings. The coatings' roughness decreases with the increase in N₂ flow rate. The hardness and modulus of elasticity increase with increasing N₂ flow. Friction and wear experiments show that the coatings' wear is mainly adhesive wear and brittle fracture. The wear debris is composed of columnar particles and a flake structure. Comprehensive analysis shows that the introduction of nitrogen can reduce the coatings' roughness and improve the mechanical and tribological properties of the coatings.

Author Contributions: Designed and performed the experiments, R.C.; writing—review and editing, Y.X., H.C. and H.L.; supervision, Y.X. All authors have read and agreed to the published version of the manuscript.

Funding: This research was funded by the National Key R&D Program of China (grant no. 2021YFB3400401) and the National Defense Industrial Technology Development Program (grant no. JCKY2018419C101).

Institutional Review Board Statement: Not applicable.

Informed Consent Statement: Not applicable.

Data Availability Statement: Not applicable.

Conflicts of Interest: The authors declare no conflict of interest.

References

1. Comello, S.; Reichelstein, S.; Sahoo, A. The road ahead for solar PV power. *Renew. Sustain. Energy Rev.* **2018**, *92*, 744–756. [[CrossRef](#)]
2. Connolly, D.; Lund, H.; Mathiesen, B.; Leahy, M. A review of computer tools for analysing the integration of renewable energy into various energy systems. *Appl. Energy* **2010**, *87*, 1059–1082. [[CrossRef](#)]
3. Yang, H.M. Simple deterministic models and applications: Comment on “Coupled disease-behavior dynamics on complex networks: A review” by Z. Wang et al. *Phys. Life Rev.* **2015**, *15*, 35–36. [[CrossRef](#)] [[PubMed](#)]
4. Said, S.A.; Al-Aqeeli, N.; Walwil, H.M. The potential of using textured and anti-reflective coated glasses in minimizing dust fouling. *Sol. Energy* **2015**, *113*, 295–302. [[CrossRef](#)]
5. Quan, Y.Y.; Zhang, L.Z. Experimental investigation of the anti-dust effect of transparent hydrophobic coatings applied for solar cell covering glass. *Sol. Energy Mater. Sol. Cells* **2017**, *160*, 382–389. [[CrossRef](#)]
6. Sarver, T.; Al-qaraghuli, A.; Kazmerski, L.L. A comprehensive review of the impact of dust on the use of solar energy: History, investigations, results, literature, and mitigation approaches. *Renew. Sustain. Energy Rev.* **2013**, *22*, 698–733. [[CrossRef](#)]
7. Fountoukis, C.; Figgis, B.; Ackermann, L.; Ayoub, M.A. Effects of atmospheric dust deposition on solar PV energy production in a desert environment. *Sol. Energy* **2018**, *164*, 94–100. [[CrossRef](#)]
8. Marzband, M.; Ghadimi, M.; Sumper, A.; Domínguez-García, J.L. Experimental validation of a real-time energy management system using multi-period gravitational search algorithm for microgrids in islanded mode. *Appl. Energy* **2014**, *128*, 164–174. [[CrossRef](#)]
9. Lu, H.; Zhao, W.J. Effects of particle sizes and tilt angles on dust deposition characteristics of a ground-mounted solar photovoltaic system. *Appl. Energy* **2018**, *220*, 514–526. [[CrossRef](#)]
10. Song, J.; Zhao, Y.; Sun, L.; Luo, Q.; Xu, H.; Wang, C.; Xin, H.; Wu, W.; Ma, F. VO₂/ATO nanocomposite thin films with enhanced solar modulation and high luminous transmittance for smart windows. *Ceram. Int.* **2022**, *48*, 15868–15876. [[CrossRef](#)]
11. Nie, B.; Wang, C.; Li, X.; Tian, H.; Chen, X.; Liu, G.; Qiu, Y.; Shao, J. High-Performance Transparent and Conductive Films with Fully Enclosed Metal Mesh. *ACS Appl. Mater. Interfaces* **2021**, *13*, 40806–40816. [[CrossRef](#)] [[PubMed](#)]
12. Xu, J.; Luo, H.; Ju, H.; Yu, L.; Zhou, G. Microstructure, mechanical and tribological properties of TaWN composite films. *Vacuum* **2017**, *146*, 246–251. [[CrossRef](#)]
13. Yan, Z.; Jiang, D.; Gao, X.; Hu, M.; Wang, D.; Fu, Y.; Sun, J.; Feng, D.; Weng, L. Friction and wear behavior of TiN films against ceramic and steel balls. *Tribol. Int.* **2018**, *124*, 61–69. [[CrossRef](#)]
14. Yin, X.; Jin, J.; Chen, X.; Ma, T.; Zhang, C. A New Pathway for Superlubricity in a Multilayered MoS₂-Ag Film under Cryogenic Environment. *Nano Lett.* **2021**, *21*, 10165–10171. [[CrossRef](#)]
15. Ji, Z.; Lin, Q.; Huang, Z.; Chen, S.; Gong, P.; Sun, Z.; Shen, B. Enhanced lubricity of CVD diamond films by in-situ synthetization of top-layered graphene sheets. *Carbon* **2021**, *184*, 680–688. [[CrossRef](#)]
16. Zaman, A.; Meletis, E.I. Microstructure and Mechanical Properties of TaN Thin Films Prepared by Reactive Magnetron Sputtering. *Coatings* **2017**, *7*, 209. [[CrossRef](#)]
17. Chen, R.; Tu, J.; Liu, D.; Yu, Y.; Qu, S.; Gu, C. Structural and mechanical properties of TaN/a-CN_x multilayer films. *Surf. Coat. Technol.* **2012**, *206*, 2242–2248. [[CrossRef](#)]
18. Asempah, I.; Xu, J.; Yu, L.; Wang, L. Effect of boron concentration on the mechanical, tribological and corrosion properties of Ta-B-N films by reactive magnetron sputtering. *Ceram. Int.* **2019**, *45*, 19395–19403. [[CrossRef](#)]
19. Serna-Manrique, M.D.; Escobar-Rincón, D.; Ospina-Arroyave, S.; Pineda-Hernández, D.A.; García-Gallego, Y.P.; Restrepo-Parra, E. Growth Mechanisms of TaN Thin Films Produced by DC Magnetron Sputtering on 304 Steel Substrates and Their Influence on the Corrosion Resistance. *Coatings* **2022**, *12*, 979. [[CrossRef](#)]
20. Lv, Q.; Huang, M.; Zhang, S.; Deng, S.; Gong, F.; Wang, F.; Pan, Y.; Li, G.; Jin, Y. Effects of Annealing on Residual Stress in Ta₂O₅ Films Deposited by Dual Ion Beam Sputtering. *Coatings* **2018**, *8*, 150. [[CrossRef](#)]
21. Sekhar, M.C.; Reddy, N.N.K.; Akkera, H.S.; Reddy, B.P.; Rajendar, V.; Uthanna, S.; Park, S.-H. Role of interfacial oxide layer thickness and annealing temperature on structural and electronic properties of Al/Ta₂O₅/TiO₂/Si metal-insulator-semiconductor structure. *J. Alloys Compd.* **2017**, *718*, 104–111. [[CrossRef](#)]
22. Shang, P.; Xiong, S.; Li, L.; Tian, D.; Ai, W. Investigation on thermal stability of Ta₂O₅, TiO₂ and Al₂O₃ coatings for application at high temperature. *Appl. Surf. Sci.* **2013**, *285*, 713–720. [[CrossRef](#)]
23. Ren, W.; Yang, G.-D.; Feng, A.-L.; Miao, R.-X.; Xia, J.-B.; Wang, Y.-G. Annealing effects on the optical and electrochemical properties of tantalum pentoxide films. *J. Adv. Ceram.* **2021**, *10*, 704–713. [[CrossRef](#)]
24. Huang, H.-L.; Chang, Y.-Y.; Chen, H.-J.; Chou, Y.-K.; Lai, C.-H.; Chen, M.Y.C. Antibacterial properties and cytocompatibility of tantalum oxide coatings with different silver content. *J. Vac. Sci. Technol. A* **2014**, *32*, 02B117. [[CrossRef](#)]
25. Horandghadim, N.; Khalil-allafi, J.; Urgen, M. Influence of tantalum pentoxide secondary phase on surface features and mechanical properties of hydroxyapatite coating on NiTi alloy produced by electrophoretic deposition. *Surf. Coat. Technol.* **2020**, *386*, 125458. [[CrossRef](#)]
26. Chao, R.; Cai, H.; Li, H.; Xue, Y. Effect of Nitrogen Flow Rate on Microstructure and Optical Properties of Ta₂O₅ Coatings. *Coatings* **2022**, *12*, 1745. [[CrossRef](#)]
27. Shasha, Y.; Feng, Y.; Minghui, C.; Yunsong, N.; Shenglong, Z.; Fuhui, W. Effect of Nitrogen doping on microstructure and wear resistance of Ta coatings deposited by direct current magnetron sputtering. *J. Met.* **2019**, *55*, 308–316. [[CrossRef](#)]
28. Xu, S.; Xu, J.; Munroe, P.; Xie, Z.-H. Nanoporosity improves the damage tolerance of nanostructured tantalum nitride coatings. *Scr. Mater.* **2017**, *133*, 86–91. [[CrossRef](#)]